

Reliable and Repeatable Power Measurements in DVB-T Systems

Leopoldo Angrisani¹, Domenico Capriglione²,
Luigi Ferrigno² and Gianfranco Miele²

¹*Dept. of Computer Science and Control Systems, University of Naples Federico II
via Claudio 21, 80125 Napoli,*

²*Dept. of Automation, Electromagnetism, Information Engineering and Industrial
Mathematics, University of Cassino,
via G. Di Biasio, 43 03043 Cassino (Fr),
Italy*

1. Introduction

Development and diffusion of digital video broadcasting (DVB) standards have revolutionized the television transmission; whether via satellite (DVB-S), via cable (DVB-C), or terrestrial (DVB-T), the number of services it can offer is able to satisfy the expectation of more demanding customers (ETSI, 2004), (Fischer, 2004). Since many countries in the world suffer from poor coverage of satellite and cable TV, DVB-T is playing a more significant role with respect to the other standards. DVB-T broadcasting networks are, in fact, growing very rapidly. A consequent and pressing need of performance assessment and large scale monitoring of DVB-T systems and apparatuses is thus posed. To reach this goal, a new set of measurements is required and a large number of parameters has to be taken into account, especially due to the complexity characterizing the DVB-T modulation process.

European Telecommunications Standards Institute (ETSI) specifies the parameters and quantities to be measured, and recommends the procedures to be adopted as well as test beds and laboratory equipments to be arranged (ETSI, 2004-2). Power measurement is, in particular, of primary concern: radiofrequency (RF) and intermediate frequency (IF) signal power, noise power, RF and IF power spectrum, should be measured as accurately as possible. Many advantages are connected with this practice, such as better optimization of transmitted power level, thus avoiding waste of energy and reducing the probability of interference with other systems that operate in the same coverage area, and reliable estimation of radiated emissions for verifying compliance limits applied in the regions of interest. Moreover, ETSI suggests the type of instrument to be used for power measurement, such as spectrum analyzer or power meter equipped with a proper sensor and a band-pass filter suitably tuned to the DVB-T frequency band. The former has to be equipped with a specific personality addressed to the integration of the input signal power spectrum on a certain frequency range (channel power measurement), the latter allows only peak and average power to be measured.

Several types of spectrum analyzer and power meter are available on the market. Most of them are general-purpose instruments, and not specifically designed to analyze DVB-T

signals. They exhibit relevant accuracy and repeatability problems in the presence of noise-like signals characterized by high peak to average power ratio (PAR), like DVB-T signals. In addition, they are not suited for large scale monitoring of DVB-T networks, where small size, light weight and low cost are critical constraints.

To give an answer to the cited needs, the scientific community has focused the attention on the definition and implementation of new digital signal processing (DSP) based methods for power measurement in DVB-T systems (Angrisani et al., 2006), (Angrisani et al., 2007), (Angrisani et al., 2008), (Angrisani et al., 2009). In particular, the methods based on power spectral density (PSD) estimators have seemed to be the most appropriate. They exploit straightforward measurement algorithms working on the achieved PSD to provide the desired value of the parameter or quantity of interest. Both non-parametric and parametric estimation algorithms have been considered. An overview of their performance in terms of metrological features, computational burden and memory needs if implemented on a real DSP hardware architecture is given hereinafter.

2. Power measurement in DVB-T systems

For assessing the performance of DVB-T systems and apparatuses, a new set of measurements is required. Many parameters and quantities have, in fact, to be evaluated, pointed out by ETSI in the ETSI TR 101 290 technical report (ETSI, 2004-2), called Digital Video Broadcasting Measurements (DVB-M). ETSI also recommends the procedures to be adopted for arranging test-beds or measurement systems.

A list of the measurement parameters and quantities defined for the DVB-T OFDM environment is shown in Table 1, and full referenced in (ETSI, 2004-2). All of them are keys for evaluating the correct operation of DVB-T systems and apparatuses, and each of them is addressed to a specific purpose. The technical report describes this purpose, where the parameter or the quantity has to be evaluated and in which manner. For the sake of clarity, it reports a schematic block diagram of a DVB-T transmitter and receiver, in which all the measurement interfaces are marked with a letter.

As it can clearly be noted from Table 1, power measurement is of great concern. RF and intermediate frequency (IF) signal power, noise power as well as RF and IF power spectrum are, in fact, relevant quantities to be measured as accurately as possible.

There are several RF power measurement instruments available in the market. They can be divided in two main categories: power meters and spectrum analyzers. Even though suggested by (ETSI, 2004-2), all of them suffer from a number of problems when measuring the power of a noise-like signal with a high PAR, as the DVB-T signal. The problems may dramatically worsen if the measurement is carried out in the field and with the aim of a large scale monitoring.

With regard to power meters, they are typically wideband instruments, and as such they must be connected to one or more calibrated band-pass filters centered at the central frequency of the DVB-T signals to be measured and with an appropriate bandwidth. Moreover, their metrological performance strongly depends on the power sensor they rely on. Several power sensors designed to measure different parameters and characterized by different frequency ranges are available on the market. Even though the choice is wide, not all power sensors are suitable to operate with signals characterized by a high PAR, as explained in (Agilent, 2003).

Measurement parameter	T	N	R
RF frequency accuracy (precision)	X		
Selectivity			X
AFC capture range			X
Phase noise of local oscillators	X		X
RF/IF signal power	X		X
Noise power			X
RF and IF spectrum	X		
Receiver sensitivity/ dynamic range for a Gaussian channel			X
Equivalent Noise Degradation (END)			X
Linearity characterization (shoulder attenuation)	X		
Power efficiency	X		
Coherent interferer			X
BER vs. C/N ratio by variation of transmitter power	X		X
BER vs. C/N ratio by variation of Gaussian noise power	X		X
BER before Viterbi (inner) decoder			X
BER before RS (outer) decoder			X
BER after RS (outer) decoder			X
I/Q analysis	X		X
Overall signal delay	X		
SFN synchronization		X	
Channel characteristics		X	

Table 1. DVB-T measurement parameters and their applicability

Differently from power meters, spectrum analyzers are narrowband instruments, and they are characterized by a more complex architecture. They allow different measurements on different RF signals. Their performance depends on several parameters like the resolution bandwidth (RBW), video bandwidth (VBW), detectors, etc. In particular, the detectors play a very important role because they can emphasize some signal characteristics giving unreliable measurement results. This is especially true when the signals involved are noise-like, as the DVB-T signal. To mitigate this problem, some suggestions described in (Agilent, 2003-2) can be followed.

In many cases, power meters and spectrum analyzers are expressly designed to be used only in laboratories; their performance drastically reduces when used in other environments, especially in the field. But, the fundamental problem that can limit their use is their cost. The total financial investment turns to be prohibitive for any interested company if a great number of instruments is needed, as when a large scale monitoring of DVB-T systems and apparatuses has to be pursued.

3. Nonparametric estimation for power measurement in DVB-T systems

In this chapter the most widely used correlation and spectrum estimation methods belonging to the nonparametric techniques, as well as their properties, are presented. They

do not assume a particular functional form, but allow the form of the estimator to be determined entirely by the data. These methods are based on the discrete-time Fourier transform of either the signal segment (direct approach) or its autocorrelation sequence (indirect approach). Since the choice of an inappropriate signal model will lead to erroneous results, the successful application of parametric techniques, without sufficient a priori information, is very difficult in practice. In the following two major nonparametric algorithms for PSD estimation have been taken into account (Angrisani L. et al., 2003). The first is based on the Welch method of averaged periodograms, which is also known as the WOSA estimator; the second applies wavelet thresholding techniques to the logarithm of the multitaper estimator.

3.1 WOSA Estimator

The WOSA estimator is computationally one of the most efficient methods of PSD estimation, particularly for long data records (Jokinen H. et al., 2000). This method is based on the division of the acquired signal $x(n)$ into smaller units called segments, which may overlap or be disjoint. The samples in a segment are weighted through a window function to reduce undesirable effects related to spectral leakage. For each segment, a periodogram is calculated.

$$S_x^i(f) = \frac{T_s}{N_s U} \left| \sum_{n=0}^{N_s-1} x^i(n) \omega(n) e^{-j2\pi f n T_s} \right|^2 \quad (1)$$

Variable f stands for frequency, $x^i(n)$ are the samples of the i -th segment, $\omega(n)$ accounts for the window coefficients, N_s denotes the number of samples in a segment, U is a coefficient given by

$$U = \frac{1}{N_s} \sum_{n=0}^{N_s-1} \omega^2(n) \quad (2)$$

and is used to remove the window effect from the total signal power, and T_s represents the sampling period. The PSD estimate $S_x(f)$ is then computed by averaging the periodogram estimates

$$S_x(f) = \frac{1}{K} \sum_{i=0}^{K-1} S_x^i(f) \quad (3)$$

where K represents the number of segments and is given by

$$K = \frac{N - N_s}{N_s - N_p} + 1 \quad (4)$$

where N stands for the total number of acquired samples, and N_p is the number of the overlapped samples between two successive segments. Overlap ratio r is defined as the percentage of ratio between the number of the overlapped samples and the number of samples in a segment, i.e.,

$$r = 100 \frac{N_p}{N_s} \% \tag{5}$$

It is worth noting that proper use of the WOSA estimator imposes the optimal choice of two parameters: 1) window function $\omega(\cdot)$ and 2) overlap ratio r . The periodogram in (2) can be easily evaluated over a grid of equally spaced frequencies through a standard fast Fourier transform (FFT) algorithm (Welch P. D. 1967).

3.2 Multitaper estimation and wavelet thresholding

The idea is to calculate a certain number H of PSD estimates, each using a different window function, which is also called data taper and applied to the whole acquired signal, and then to average them together (Moulin P., 1994). If all data tapers are orthogonal, the resulting multitaper estimator can exhibit good performance, in terms of reduced bias and variance, particularly for signals characterized by a high dynamic range and/or rapid variations, such as those that are peculiar to DVB-T systems.

The multitaper estimator has the following form:

$$S_x(f) = \frac{1}{H} \sum_{i=0}^{H-1} S_x^i(f) \tag{6}$$

where the terms $S_x^i(f)$ called eigenspectra are given by

$$S_x^i(f) = \left| \sum_{n=0}^{N-1} x(n) h_i(n) e^{-j2\pi f n T_s} \right| \tag{7}$$

where $\{h_i(n) : n = 0, \dots, N-1; i=1, \dots, H\}$ denotes a set of orthonormal data tapers. A convenient set of easily computable orthonormal data tapers is the set of sine tapers, the i^{th} of which is

$$h_i(n) = \left(\frac{2}{N+1} \right)^{1/2} \sin \left(\frac{(i+1)\pi n}{N+1} \right). \tag{8}$$

A standard FFT algorithm proves to be appropriated in evaluating the eigenspectra over a grid of equally spaced frequencies (Walden et al., 1998).

Provided that H is equal to or greater than 5, it can be demonstrated that random variable $\eta(f)$, as given by

$$\eta(f) = \log \frac{S_x(f)}{S(f)} - \psi(H) + \log H \tag{9}$$

has Gaussian distribution with zero mean and variance σ^2_η equal to $\psi'(H)$; $S(f)$ represents the true PSD, and $\psi(\cdot)$ and $\psi'(\cdot)$ denote the digamma and trigamma functions, respectively (Moulin P., 1994). If we let

$$Y(f) = \log S_x(f) - \psi(H) + \log H \tag{10}$$

we have

$$Y(f) = \log S(f) + \eta(f) \tag{11}$$

i.e., the logarithm of the multitaper estimator, plus a known constant, can be written as the true log spectrum plus approximately Gaussian noise with zero mean value and known variance σ_η^2 .

These conditions make wavelet thresholding techniques particularly suitable to remove noise and, thus, to produce a smooth estimate of the logarithm of the PSD. In particular, after evaluating the discrete wavelet transform (DWT) of $Y(f)$ computed according to (10), the resulting wavelet coefficients, which are also Gaussian distributed, can be subjected to a thresholding procedure, and the aforementioned smooth estimate can be obtained by applying the inverse DWT to the thresholded coefficients (Walden et al., 1998). A soft threshold function $\delta(\alpha, T)$ is suggested, and it is defined by

$$\delta(\alpha, T) = \text{sgn}(\alpha) \begin{cases} |\alpha| - T, & \text{if } |\alpha| > T \\ 0, & \text{otherwise} \end{cases} \quad (12)$$

where α denotes the generic wavelet coefficient, and T is the threshold level. In (Donoho D. L. & Johnstone I. M., 1994), Donoho and Johnstone demonstrated that, in the presence of Gaussian noise with zero mean value and variance σ_η^2 , the optimal value of T is

$$T = \sigma_\eta \sqrt{2 \times \log N} \quad (13)$$

where N , which is the number of samples, must be of power of two.

In addition, in this case, the right choice of two parameters, i.e., the number of data tapers H and the mother wavelet $\zeta(\cdot)$ for DWT and inverse DWT evaluation, has to be made to gain a sound spectral estimation.

3.3 Performance optimization and assessment

To optimally choose window function $\omega(\cdot)$ and overlap ratio r for the WOSA estimator and the number of data tapers H and mother wavelet $\zeta(\cdot)$ for the multitaper estimator, a suitable simulation stage has been designed. Regarding r , all values ranging from 0% up to 90%, with a step of 10%, have been considered. As for $\omega(\cdot)$, a large set of functions, which differ from one another in relevant spectral characteristics, has been arranged; the set includes most windows defined in (Reljin I. et al., 1998), such as Hanning, Blackman, MS-3FT, MS-4FT, FD-3FT, and FD-4FT, and the new window proposed in (Jokinen H. et al., 2000), which is referred to as Ollila. Concerning H , the considered values range from 5 up to 50, with a step of 5. In addition, various mother wavelets characterized by different vanishing moments (db3, db8, sym3, sym8, coif1, coif5, bior2.2, and bior2.8) have been enlisted (Daubechies I., 1992).

A number of numerical tests have, in particular, been executed in the Matlab 7 environment, with the aim of minimizing the following figures of merit:

1. experimental standard deviation characterizing both total (σ_T) and channel (σ_C) power measurement results;
2. difference between the mean value of the results provided by the method and the imposed value, which is considered as reference, for both total (Δ_T) and channel (Δ_C) power.

The channel power is obtained by integrating the PSD over the frequency interval that is centered at the tune frequency and as wide as the nominal spacing of the channel itself

(ETSI, 2004). Instead the total power is evaluated integrating the PSD over the whole frequency span analyzed from zero up to half of the adopted sample rate f_s ($f_s=1/T_s$). DVB-T reference signals have first been generated. To this aim, the analytical expression for the PSD of a DVB-T signal given by

$$S_x(f) = \sum_{k=-(K-1)/2}^{(K-1)/2} \left[\frac{\sin(\pi(f-f_k)(\Delta+T_u))}{\pi(f-f_k)(\Delta+T_u)} \right]^2 \quad f_k = f_c + \frac{k}{T_u} \quad (14)$$

has been considered, where f_c is the RF signal central frequency, K is the number of transmitted carriers, Δ is the duration of the guard interval, and T_u is the time duration of the useful part of a DVB-T symbol (the useful part does not include the guard interval) (ETSI, 2004). Moreover, the approximate method in the frequency domain presented in (Percival D. B., 1992) has been adopted. It assures accurate time-domain realizations of a zero-mean Gaussian process, which is characterized by a known PSD.

The following DVB-T transmission settings have been imposed: 8K transmission mode ($K=6817$ and $T_u=896 \mu s$) and $1/4$ ($\Delta=224 \mu s$) and $1/32$ ($\Delta=28 \mu s$) guard intervals. In addition, three values of the oversampling factor (considered as the ratio between the sample rate and the RF signal central frequency) have been simulated, and the hypothesis of the acquired records covering one DVB-T symbol has been held. For each transmission setting and oversampling factor value, 50 different realizations (test signals) have been produced.

The obtained results are given in Tables 2 and 3 for the multitaper and WOSA estimators, respectively. Each pair of round brackets describes the couple ($\zeta(\cdot) - H$ or $\omega(\cdot) - r$) that minimizes the related figure of merit. The last row of both tables quantifies the computation burden in terms of mean processing time on a common Pentium IV computer.

From the analysis of the results, some considerations can be drawn.

- Both estimators have assured good repeatability; the experimental standard deviation is always lower than 0.20%.
- Repeatability improves upon the widening of the guard interval, and the oversampling factor seems to have no influence.
- The WOSA estimator exhibits better performance in terms of Δ_T and Δ_C .
- Measurement time peculiar to the multitaper estimator is much longer than that taken by the WOSA estimator.

The WOSA estimator has given a better trade-off between metrological performance and measurement time, thus confirming the outcomes presented in (Angrisani L. et al., 2006). This is the reason the multitaper estimator has no longer been considered in the subsequent stages of the work.

To fix the minimum hardware requirements of the data acquisition system (DAS) to be adopted in the experiments on emulated and actual DVB-T signals described in the succeeding sections, further tests have been carried out. The sensitivity of the proposed method to the effective number of bits (ENOB) and acquired record length has been assessed. The obtained results are given in Figs. 1 and 2; they refer to a guard interval equal to $224 \mu s$. In particular, Fig. 1 shows the values of σ_C [Fig. 1(a)], Δ_C [Fig. 1(b)], and Δ_T [Fig. 1(c)] versus ENOB for three values of the oversampling factor; Fig. 1(d) presents the estimated PSD for the considered values of ENOB. With regard to σ_T , values very similar to those characterizing σ_C have been experienced. Fig. 2 shows the values of σ_T [Fig. 2(a)] and Δ_T [Fig. 2(b)] versus the acquired record length for the same values of the oversampling factor. With regard to σ_C and Δ_C , values very similar to those characterizing σ_T and Δ_T , respectively, have been experienced.

Figure of merit	Guard interval [μ s]	Oversampling factor		
		~ 3	~ 6	~ 12
σ_r [%]	28	0,148 (sym8,10)	0,176 (db3,25)	0,151 (db3,25)
	224	0,129 (coif1,50)	0,097 (coif1,50)	0,117 (db3,25)
σ_c [%]	28	0,148 (sym8,10)	0,176 (db3,25)	0,151 (db3,25)
	224	0,129 (coif1,50)	0,097 (coif1,50)	0,117 (db3,25)
Δ_r [%]	28	0,1104 (bior2.8,50)	0,1252 (bior2.8,50)	0,6335 (bior2.8,50)
	224	0,1509 (bior2.8,50)	0,1050 (bior2.8,50)	0,1237 (bior2.8,50)
Δ_c [%]	28	0,1105 (bior2.8,50)	0,1253 (bior2.8,50)	0,6336 (bior2.8,50)
	224	0,1509 (bior2.8,50)	0,1050 (bior2.8,50)	0,1238 (bior2.8,50)
Measurement time [s]	28	12,55	59,46	280,53
	224	53,61	280,58	1168,20

Table 2. Results obtained in the simulation stage: multitaper estimator is involved.

Figure of merit	Guard interval [μ s]	Oversampling factor		
		~ 3	~ 6	~ 12
σ_r [%]	28	0,149 (Ollila,70)	0,181 (Ollila,50)	0,148 (Ollila,30)
	224	0,130 (blackman,60)	0,098 (hanning,50)	0,092 (Ollila,50)
σ_c [%]	28	0,149 (Ollila,70)	0,181 (Ollila,50)	0,148 (Ollila,30)
	224	0,130 (blackman,60)	0,098 (hanning,50)	0,092 (Ollila,50)
Δ_r [%]	28	0,0015 (FD3FT,30)	5,4091e-4 (FD3FT,30)	0,0017 (FD4FT,60)
	224	0,0068 (blackman,40)	0,0028 (MS3FT,10)	0,0020 (MS4FT,60)
Δ_c [%]	28	0,0015 (FD3FT,30)	6,0611e-4 (FD3FT,30)	0,0012 (FD4FT,60)
	224	0,0068 (blackman,40)	0,0017 (MS3FT,10)	0,0020 (MS4FT,60)
Measurement time [s]	28	0,032	0,052	0,096
	224	0,053	0,094	0,177

Table 3. Results obtained in the simulation stage: WOSA estimator is involved.

Looking at Fig. 1, it is possible to establish that 1) an ENOB equal to or greater than six grants an experimental standard deviation in both total (σ_T) and channel (σ_C) power measurements of less than 0.15%, and 2) Δ_C does not seem to be affected by vertical quantization, as, on the contrary, Δ_T does. Furthermore, Fig. 2 clearly evidences that σ_T improves upon the widening of the record length, whereas satisfying values of Δ_T can be achieved if the record lengths covering greater than one half of the DVB-T symbol are considered.

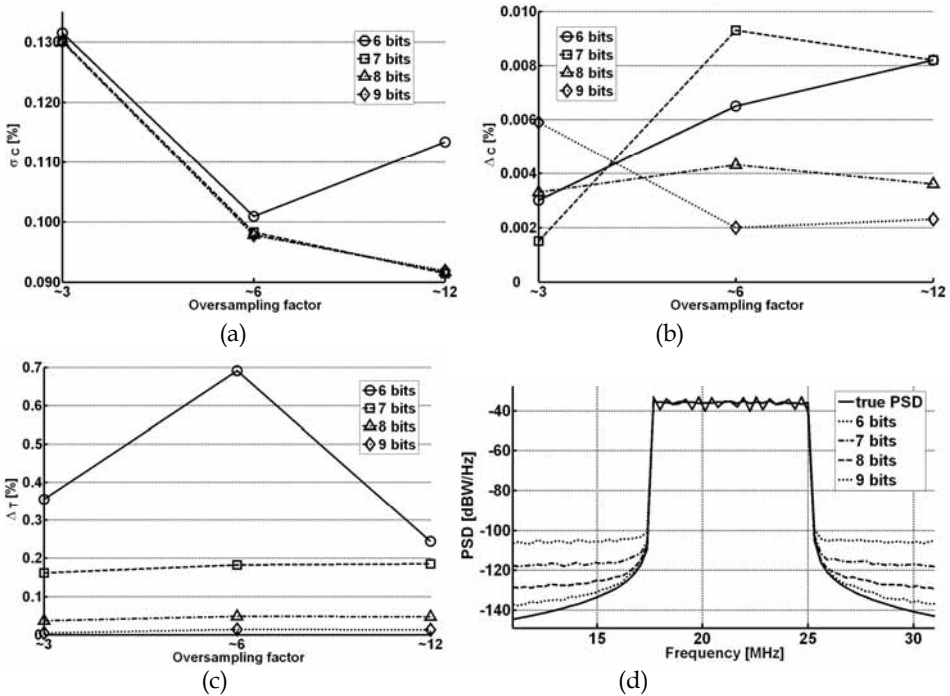


Fig. 1. Simulation stage: a) σ_C , b) Δ_C , and c) Δ_T versus ENOB for three values of the oversampling factor; d) estimated PSD for the considered values of ENOB.

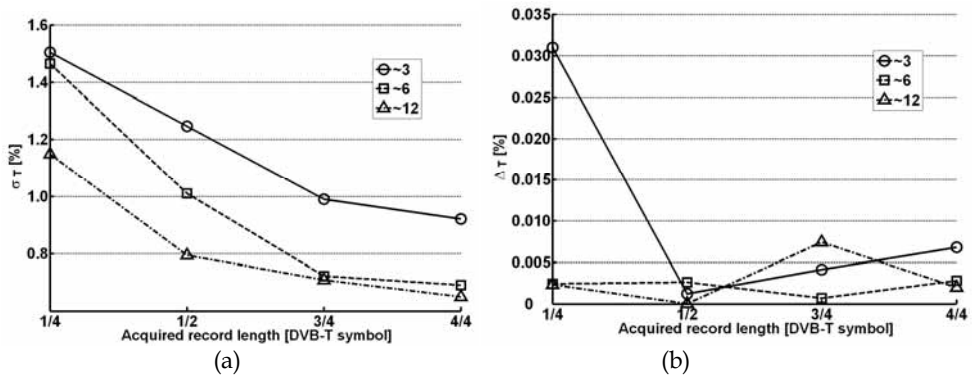


Fig. 2. Simulation stage: a) σ_T and b) Δ_T versus acquired record length for three values of the oversampling factor.

These considerations match well with the typical characteristics of the data acquisition systems available on the market today. High values of the sample rate, required to optimally acquire RF or IF DVB-T signals, are often associated with ENOB not lower than 6 bits.

Further an emulation stage has been designed and applied, with the aim of assessing the performance of the proposed method in the presence of a real DAS and comparing it with that assured by competitive measurement solutions that are already available on the market. Stemming from past experience documented in (Angrisani L. et al., 2006), a suitable measurement station, which is sketched in Fig. 3, has been set up. It has included the following: 1) a processing and control unit, i.e., a personal computer, on which the measurement algorithm has run; 2) an RF signal generator equipped with DVB-T personalities Agilent Technologies E4438C (with an output frequency range of 250 kHz–6 GHz); 3) a traditional spectrum analyzer [express spectrum analyzer (ESA)] Agilent Technologies E4402B (with an input frequency range of 9 kHz–3 GHz); 4) a VSA Agilent Technologies E4406A (with an input frequency range of 7 MHz–4 GHz); 5) a real-time spectrum analyzer (RSA) Tektronix RSA3408A (with an input frequency range of dc–8 GHz); 6) an RF power meter (PM) Agilent Technologies N1911A equipped with two probes N1921A (with an input frequency range of 50 MHz–18 GHz) and E9304A (with an input frequency range of 6 kHz–6 GHz); and 7) a DAS LeCroy SDA6000A (with 6-GHz bandwidth and 20-GS/s maximum sample rate). They are all interconnected through an IEEE-488 interface bus. The function generator has provided 8-MHz-bandwidth DVB-T test signals characterized by an RF central frequency equal to 610 MHz, a nominal total power of -20 dBm, and a 64-state quadrature amplitude modulation (QAM) scheme. Moreover, the same transmission settings considered in the previous stage have been imposed.



Fig. 3. Measurement station for performance assessment.

A preliminary characterization of cables and connectors utilized in the measurement station has been carried out through the vector network analyzer ANRITSU 37347C (with an input frequency range of 40 MHz–20 GHz), which is equipped with a 3650 SMA 3.5-mm calibration kit (Anritsu, 2003). The mean value and experimental standard deviation of 100 attenuation measures obtained in the interval of 606–614 MHz are given in Table 4.

	Mean attenuation	Experimental standard deviation
Power meter	0.829150	0.000039
Spectrum analyzers	0.834860	0.000019
Oscilloscope	0.834140	0.000014

Table 4. Characterization results of cables and connectors utilized in the measurement station of Fig. 3.

Different operative conditions of the DAS, in terms of vertical resolution (7 and 8 bits nominal) and observation period (1/4, 1/2, 3/4, and 1 DVB-T symbol), have been considered. For each operative condition and transmission setting, 50 sample records have been acquired and analyzed through the proposed method. Examining the obtained results given in Table 5 and Fig. 4, it can be noted that two conditions hold.

1. Higher sampling factors do not seem to affect the method’s metrological performance; the same is true if vertical resolution is considered.
2. Performance enhancement can be noticed both in the presence of acquired records covering increasingly longer observation periods.

Successively, 50 repeated measurements of total and channel power have been executed by means of PM and spectrum analyzers (ESA, VSA, and RSA), respectively. Table 6 accounts for the results provided by the PM, whereas Table 7 enlists those that are peculiar to the analyzers. As an example, Fig. 5 sketches a typical PSD estimated by the proposed method [Fig. 5(a)], ESA [Fig. 5(b)], VSA [Fig. 5(c)], and RSA [Fig. 5(d)].

With regard to total power, three considerations can be drawn.

1. Results furnished by the PM are different for the two probes adopted.
2. Experimental standard deviation peculiar to the PM is slightly better than that assured by the proposed method.
3. PM outcomes concur with the total power measurement results of the proposed method; a confidence level equal to 99% is considered (Agilent, 2005).

As for the channel power, it is worth stressing that two conditions hold.

1. The proposed method exhibits satisfying repeatability. The related experimental standard deviation is better than that characterizing ESA, VSA, and RSA results.

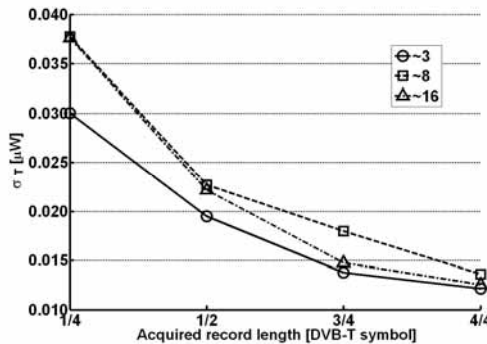


Fig. 4. Emulation stage: σ_T versus acquired record length for three values of the oversampling factor.

8k transmission mode, 64-QAM modulation scheme, 8 bit vertical resolution				
Figure of Merit	Guard Interval [μ s]	Oversampling factor		
		~ 3	~ 8	~ 16
σ_T [μ W]	28	0.012	0.014	0.013
	224	0.0094	0.017	0.011
σ_C [μ W]	28	0.012	0.014	0.013
	224	0.0094	0.017	0.011
P_T [μ W]	28	9.931	10.024	9.937
	224	10.142	10.163	10.144
P_C [μ W]	28	9.890	9.989	9.895
	224	10.1030	10.125	10.105

8k transmission mode, 64-QAM modulation scheme, 7 bit vertical resolution				
Figure of Merit	Guard Interval [μ s]	Oversampling factor		
		~ 3	~ 8	~ 16
σ_T [μ W]	28	0.011	0.034	0.014
	224	0.011	0.029	0.015
σ_C [μ W]	28	0.011	0.032	0.014
	224	0.011	0.028	0.016
P_T [μ W]	28	10.148	10.162	10.157
	224	10.079	10.098	10.097
P_C [μ W]	28	9.971	9.985	9.980
	224	9.899	9.919	9.916

Table 5. Total and channel power measures provided by the proposed method. The acquired record covers a single DVB-T symbol.

Transmission Settings 8k, 64-QAM, 610 MHz central frequency			
PM	Guard Interval [μ s]	P_{PM} [μ W]	σ_{PM} [μ W]
N1921A PROBE	28	9.9444	0.0018
	224	9.9630	0.0020
E9304A PROBE	28	8.0402	0.0060
	224	7.95910	0.00086

Table 6. Mean values (PPM) and experimental standard deviations (σ_{PM}) of total power measures provided by the PM equipped with N1921A and E9304A probes.

2. ESA, VSA, and RSA outcomes concur with the channel power measurement results of the proposed method; a confidence level equal to 99% is considered (Agilent, 2004), (Agilent, 2001), (Tektronix, 2006).

Finally, a number of experiments on real DVB-T signals have been carried out through the optimized method. The signals have been radiated by two MEDIASET DVB-T multiplexers operating on the UHF 38 (610-MHz RF central frequency) and UHF 55 (746-MHz RF central frequency) channels, respectively.

A simplified measurement station, as sketched in Fig. 6, has been adopted. With respect to that used in the emulation stage, the function generator has been replaced by a suitable amplified antenna, the VSA and RSA have been removed, and a power splitter has been added. Cables, connectors, and a power splitter have been characterized through the

Transmission Settings: 8k, 64-QAM, 610 MHz central frequency					
Instrument	RBW [kHz]	Guard Interval [μs]	P_{SA} [μW]	σ_{SA} [μW]	
ESA	100	28	10.322	0.074	
	100	224	10.656	0.080	
	30	28	10.376	0.068	
	30	224	10.142	0.070	
VSA	0.871	28	10.506	0.036	
	0.871	224	10.218	0.023	
	30	28	10.162	0.099	
	30	224	9.52	0.12	
RSA	SPECTRUM ANALYZERS	50	28	9.311	0.044
		50	224	9.318	0.042
		30	28	9.158	0.041
		30	224	9.042	0.044
	REAL TIME MODE		28	9.177	0.097
			224	9.088	0.081

Table 7. Mean values (P_{SA}) and experimental standard deviations (σ_{SA}) of channel power measures provided by ESA, VSA and RSA; different settings of their resolution bandwidth have been considered.

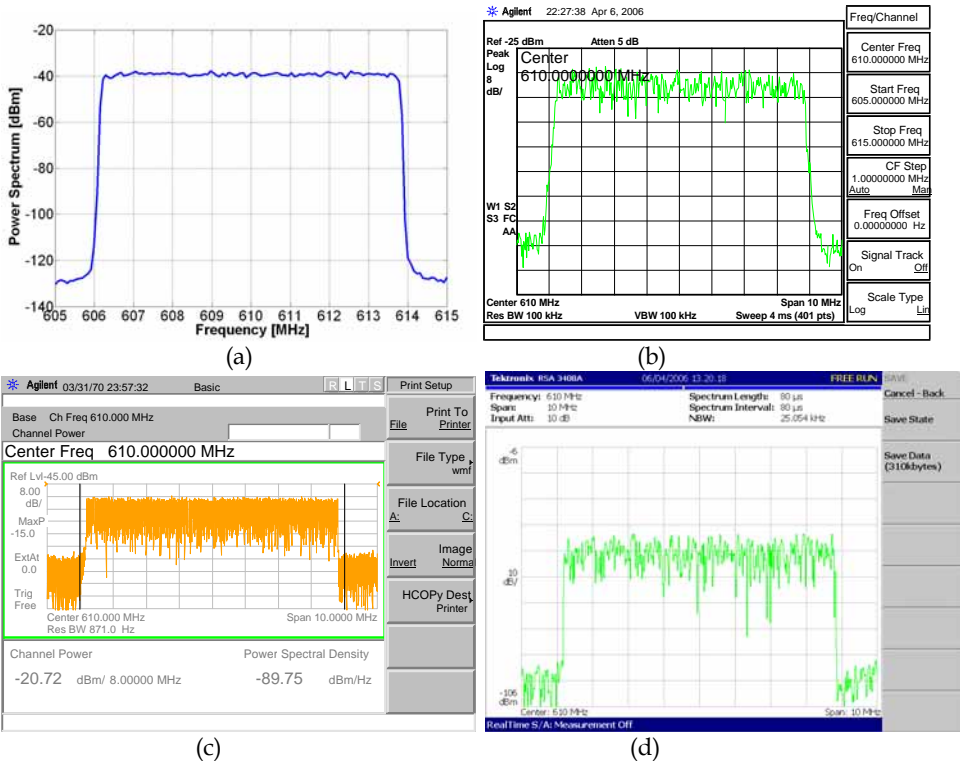


Fig. 5. Power spectrum of an emulated DVB T signal estimated by a) the proposed method, b) ESA, c) VSA and d) RSA.

forementioned vector network analyzer. The mean value and experimental standard deviation of 100 attenuation measures obtained in the UHF 38 and UHF 55 channels are given in Table 8.

As an example, Fig. 7(a) and (b) shows the power spectrum of a DVB-T signal, which is radiated by the MEDIASET multiplexer operating on UHF 55, as estimated by the proposed method and ESA, respectively. Channel power measurement results are summarized in Table 9; good agreement can be appreciated, confirming the efficacy of the proposal (Angrisani L. et al., 2008).

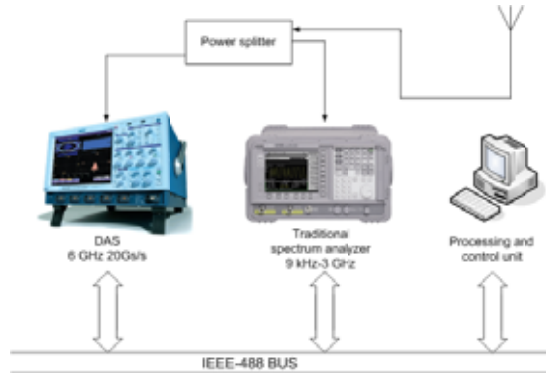


Fig. 6. Measurement station for the experiments on real DVB-T signals.

	UHF Channel	Mean attenuation [dB]	Experimental standard deviation [dB]
DAS	38	-4.703	0.032
	55	-5.403	0.042
Traditional Spectrum Analyzer	38	-19.393	0.021
	55	-19.3886	0.0086

Table 8. Characterization results of cables and connectors utilized in the measurement station of Fig. 6.

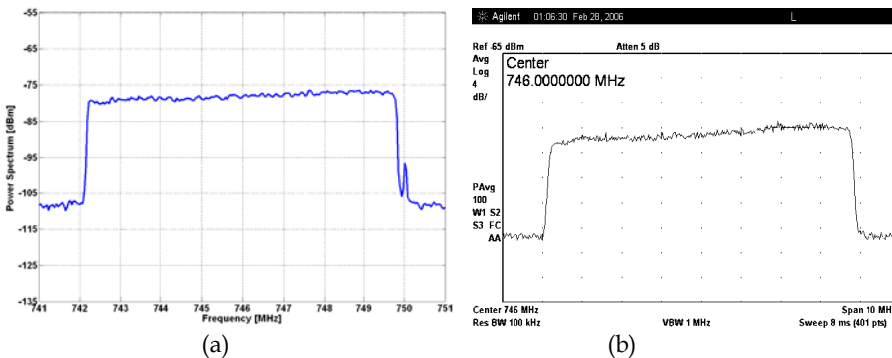


Fig. 7. Power spectrum of a real DVB T signal measured by the a) proposed method and b) ESA.

8k transmission mode, 64-QAM, 28μs guard interval		
	UHF Channel 38	UHF Channel 55
	610 MHz	746 MHz
Proposed Method	90.94 nW	93.07 nW
Traditional Spectrum Analyzer	94.06 nW	93.23 nW

Table 9. Experimental results.

4. Parametric estimation for power measurement in DVB-T systems

Parametric estimation methods suppose that the analyzed signal is the output of a model, which is represented as a linear system driven by a noise sequence ϵ_n . They evaluate the PSD of the signal by estimating the parameters (coefficients) of the linear system that hypothetically “generates” the signal. Among the various methods, autoregressive (AR) approaches are widespread. The computational burden related to AR approaches is, in fact, significantly less than that required to implement moving average (MA) or autoregressive moving average (ARMA) parameter estimation algorithms (Marple, 1980). A stationary autoregressive process of order p , i.e., AR(p), satisfies

$$x_n = - \sum_{m=1}^p a_{p,m} x_{n-m} + \epsilon_n \tag{15}$$

where $a_{p,1}, a_{p,2}, \dots, a_{p,p}$ are fixed coefficients, and $\{\epsilon_n\}$ is a white noise process with variance σ_p^2 . The PSD of the stationary process described by AR(p) is totally described by the model parameters and the variance of the white noise process. It is given by

$$S(f) = \frac{\sigma_p^2 T_s}{\left| 1 + \sum_{m=1}^p a_{p,m} e^{-j2\pi m f T_s} \right|^2} \quad |f| \leq f_N \tag{16}$$

where $T_s = 1/f_s$ is the sampling interval, and $f_N = 1/(2T_s)$ is the Nyquist frequency. Consequently, with known p , it is necessary to properly estimate the $p+1$ parameters $a_{p,1}, a_{p,2}, \dots, a_{p,p}$ and σ_p^2 . To reach this goal, the relationship between the AR parameters and the autocorrelation sequence (known or estimated) of x_n has to be fixed, as described here.

4.1 Yule–Walker equations

Achieving the expectations on the product $x_n x_{n-k}^*$, the autocorrelation sequence is evaluated as

$$R_{xx}(k) = E[x_n x_{n-k}^*] = - \sum_{m=1}^p a_{p,m} R_{xx}(k-m) + E[\epsilon_n x_{n-k}^*]. \tag{17}$$

The plausible fact that $E[\epsilon_n x_{n-k}^*] = 0$, for $k > 0$, implies that

$$\begin{aligned} E[\epsilon_n x_n^*] &= E \left[\epsilon_n \left(- \sum_{m=1}^p a_{p,m}^* x_{n-m}^* + \epsilon_n^* \right) \right] = \\ &= - \sum_{m=1}^p a_{p,m}^* E[\epsilon_n x_{n-m}^*] + \sigma_p^2 = \sigma_p^2 \end{aligned} \tag{18}$$

4.3 Forward linear prediction algorithm

In the literature, several least-squares estimation procedures that directly operate on the data to yield better AR parameter estimates can be found. These techniques often produce better AR spectra than that obtained with the Yule-Walker approach.

Assume that the sequence x_0, \dots, x_{N-1} is used to find the p -th-order AR parameter estimates. The forward linear predictor is (Makhoul, 1975)

$$\hat{x}_n = -\sum_{k=1}^p a_{p,k} x_{n-k} \tag{26}$$

It is possible now to define the forward linear prediction error

$$e_p(n) = x_n - \hat{x}_n = \sum_{k=0}^p a_{p,k} x_{n-k} \quad \text{for } p \leq n \leq N-1 \tag{27}$$

where $a_{p,0}=1$. Therefore, $e_p(n)$, for $n=p$ to $n=N-1$, can be obtained by

$$\begin{bmatrix} \overbrace{e_p(p)}^E \\ M \\ \overbrace{e_p(N-1)}^E \end{bmatrix} = \begin{bmatrix} \overbrace{x_p \quad L \quad x_0}^{X_p} \\ M \quad M \\ x_{N-1} \quad L \quad x_{N-p-1} \end{bmatrix} \begin{bmatrix} \overbrace{1}^A \\ a_{p,1} \\ M \\ a_{p,p} \end{bmatrix} \tag{28}$$

where X_p is an $(N-p) \times (p+1)$ Toeplitz matrix.

The approach followed to estimate $a_{p,k}$ consists of minimizing a sum of $e_p(n)$ called prediction error energy, i.e.,

$$SS_p = \sum_{n=p}^{N-1} |e_p(n)|^2 = \sum_{n=p}^{N-1} \left| \sum_{k=0}^p a_{p,k} x_{n-k} \right|^2 = E^H E \tag{29}$$

Using an alternative description of the $N-p$ error equation (28) such as

$$E = \begin{bmatrix} \overbrace{x_p}^{X_p} \\ y \end{bmatrix} \begin{bmatrix} \overbrace{1}^A \\ a \end{bmatrix} \tag{30}$$

where $y = [x_p, \dots, x_{N-1}]^T$, $a = [a_{p,1}, \dots, a_{p,p}]^T$, and $X = \begin{bmatrix} x_{p-1} & L & x_0 \\ M & & M \\ x_{N-2} & L & x_{N-p-1} \end{bmatrix}$ the prediction error

energy (29) may be expressed as

$$SS_p = E^H E = y^H y + y^H X a + a^H X^H y + a^H X^H X a \tag{31}$$

To minimize SS_p , this term must be set to zero (Marple, 1987), i.e.,

$$X^H y + X^H X a = 0_p, \tag{32}$$

where 0_p is the all-zeros vector, obtaining

$$SS_{p,\min} = y^H y + y^H X a. \quad (33)$$

Equations (32) and (33) may be combined into a single set of

$$\begin{aligned} \begin{bmatrix} y^H y & y^H X \\ X^H y & X^H X \end{bmatrix} \begin{bmatrix} 1 \\ a \end{bmatrix} &= \begin{bmatrix} y & X \end{bmatrix}^H \begin{bmatrix} y & X \end{bmatrix} \begin{bmatrix} 1 \\ a \end{bmatrix} = \\ &= (X_p)^H X_p \begin{bmatrix} 1 \\ a \end{bmatrix} = \begin{bmatrix} SS_{p,\min} \\ 0_p \end{bmatrix} \end{aligned} \quad (34)$$

These equations form the normal equations of the least squares analysis. This method is called the covariance method (Makhoul, 1975). Due to the particular properties of $(X_p)^H X_p$, it is possible to develop a fast algorithm that is similar to that of the Levinson algorithm. The original fast algorithm for solving the covariance normal equations was developed by Morf et al. (Morf et al, 1977), and further computational reduction was studied by Marple and reported in (Marple, 1987), producing an algorithm that requires $o(p^2)$ operations.

4.4 Burg algorithm

This is the most popular approach for AR parameter estimation with N data samples and was introduced by Burg in 1967 (Burg, 1967). It may be viewed as a constrained least-squares minimization.

The approach followed to estimate $a_{k,k}$ consists of minimizing a sum of forward and backward linear prediction error energies, i.e.,

$$SS_p = \sum_{n=p}^{N-1} \left[|e_p(n)|^2 + |b_p(n)|^2 \right] \quad (35)$$

where $e_p(n)$ is defined by (27), and $b_p(n)$ is the backward linear prediction error, which is given by

$$b_p(n) = \sum_{k=0}^p a_{p,k}^* X_{n-p+k} \quad \text{for } p \leq n \leq N-1. \quad (36)$$

Note that $a_{p,0}$ is defined as unity.

Substitution of (24) into (27) and (36) yields the following recursive relationship between the forward and backward prediction errors:

$$e_p(n) = e_{p-1}(n) + a_{p,p} b_{p-1}(n-1) \quad \text{for } p \leq n \leq N-1 \quad (37)$$

$$b_p(n) = b_{p-1}(n-1) + a_{p,p}^* e_{p-1}(n) \quad \text{for } p \leq n \leq N-1 \quad (38)$$

and substituting (37) and (38) into (35), SS_p can be written as

$$SS_p = \Gamma_p + 2a_{p,p} \Lambda_p + \Gamma_p a_{p,p}^2 \quad (39)$$

whose coefficients are

$$\Gamma_p = \sum_{n=p}^{N-1} \left[\left| e_{p-1}(n) \right|^2 + \left| b_{p-1}(n-1) \right|^2 \right] \tag{40}$$

$$\Lambda_p = 2 \sum_{n=p}^{N-1} e_{p-1}(n) b_{p-1}^*(n-1). \tag{41}$$

The value of $a_{p,p}$ that minimizes SS_p can easily be calculated by setting the derivative to zero and obtaining

$$a_{p,p} = -\frac{\Lambda_p}{\Gamma_p}. \tag{42}$$

The routine implemented to estimate the AR coefficients is shown in Fig. 2. It needs an initializing step, in which the starting value of the observed forward and backward prediction errors and the innovation variance are chosen using the following relations:

$$e_0(n) = b_0(n) = x_n \tag{43}$$

$$\sigma_0^2 = \frac{1}{N} \sum_{n=1}^N |x_n|^2. \tag{44}$$

The Burg algorithm requires a number of operations proportional to p^2 .

4.5 Forward and backward linear prediction algorithm

This approach, which was independently proposed by Ulrych and Clayton (Ulrych T. J. & Clayton R. W., 1976). and Nuttall (Nuttall A. H., 1976), is a least-squares procedure for forward and backward predictions, in which the Levinson constraint imposed by Burg is removed.

Noting that (27) and (36) can be summarized by

$$\Delta = \begin{bmatrix} E \\ B^* \end{bmatrix} = \begin{bmatrix} X_p \\ X_p^* J \end{bmatrix} \begin{bmatrix} 1 \\ a \end{bmatrix} \tag{45}$$

where $B = [b_p(p), \dots, b_p(N-1)]^T$, J is an $(p + 1) \times (p + 1)$ reflection matrix, and $X_p^* J$ is a Hankel matrix of conjugated data elements, it is possible to rewrite (35) as

$$SS_p = \Delta^H \Delta = E^H E + B^H B. \tag{46}$$

The preceding equation can be minimized with the same procedure used for the covariance method, leading to the set of normal equations

$$\overbrace{\begin{bmatrix} X_p^H & X_p^H \\ X_p^* J & X_p^* J \end{bmatrix}}^{R_p} \begin{bmatrix} 1 \\ a \end{bmatrix} = \begin{bmatrix} SS_{p,\min} \\ 0_p \end{bmatrix}. \tag{47}$$

Because the summation range in (35) is identical to that of the covariance method, this least-squares approach is called the modified covariance method. The system (47) can be solved by a matrix inversion that requires a number of operations proportional to p^3 , which is one order of magnitude greater than Burg’s solution.

Due to the characteristic of the actual structure of the matrix R_p , Marple (Marple, 1980), (Marple, 1987) suggested an algorithm requiring a number of computations proportional to p^2 .

4.6 Performance optimization and assessment

The performance of parametric power spectrum estimation methods depends on the model order p . To regulate this parameter to operate with success on DVB-T systems, a suitable simulation stage has been designed and set-up. Once the optimal value of p has been found, a first comparison with the optimized Welch method has been made. Successively further investigation has been carried out in simulation environment, with the aim of evaluating the performance of parametric spectrum estimation methods when they are applied to signals characterized by different quantization levels. Afterwards an emulation stage has been designed and applied with the aim of:

- assessing the performance of the proposed method in the presence of a real DAS;
- comparing it to that assured by competitive measurement solutions already available on the market;
- comparing it to that assured by the optimized Welch method.

Moreover a number of experiments on real DVB-T signals have been carried out through the optimized method, in order to make a comparison with the results obtained in the previous stages. At last the suitability of these methods to be implemented in a low cost DSP platform has been investigated.

As said in the previous paragraph, the performance of PSD AR estimators depends on the polynomial order p . To optimally choose this parameter, a suitable simulation stage has been designed. A number of numerical tests have been executed in the Matlab 7 environment, with the aim of minimizing the same figures of merit defined in the previous section. These tests have been carried out by adopting the same reference signals defined above.

With special regard to AR estimation algorithms, taking into account that higher values of p may introduce spurious details in the estimated spectrum and lower values of p may drive to a highly smoothed spectral estimate (Kay & Marple, 1981), a dual stage optimization procedure has been applied. In the first stage, a rough optimization has been pursued; in particular, a suitable operative range for p has been fixed. The second stage has finely tuned the value of p , within the range previously determined, through the minimization of σ_c and Δ_c .

4.6.1 Rough optimization

Suitable figures of merit, which are addressed to highlight the goodness of the PSD estimates, have been considered. Much attention has been paid to the final prediction error, Akaike's information criterion, and the root mean square error (RMSE); details can be found in (Kay & Marple, 1981) and (Angrisani L. et al., 2003).

Concerning p , two different and consecutive sets have been organized: $\Sigma_1 = \{p \mid 10 \leq p \leq 100\}$ and $\Sigma_2 = \{p \mid 100 < p \leq 5000\}$. In Σ_1 , an analysis step of 10 has been adopted, whereas a step of 100 has been considered for Σ_2 .

All tests have highlighted quite the same behavior of the three figures of merit; they have reached their minima in strictly overlapping p ranges. For the sake of brevity, Fig. 8 shows only the minimum value of RMSE [Fig. 8(a)] and the corresponding value of p [Fig. 8(b)]

versus the observation period expressed as a fraction of the time interval associated with one DVB-T symbol; a guard interval of 224 μ s and an oversampling factor of 3 have, in particular, been considered. Very similar outcomes have been attained with a guard interval of 28 μ s and two oversampling factors, which are equal to 6 and 12.

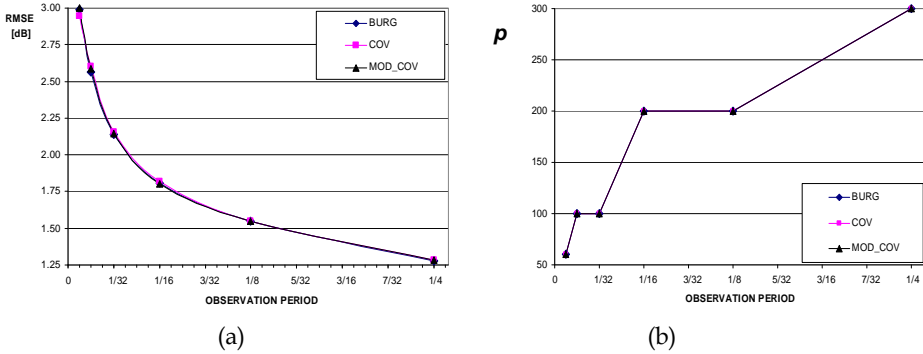


Fig. 8. a) Minimum values of RMSE and (b) corresponding values of p versus the observation period, which is expressed as a fraction of the time interval associated with one DVB-T symbol.

From the analysis of the results, some considerations have emerged.

1. The covariance, Burg, and modified covariance estimators reach the lowest RMSE for very similar values of the polynomial order p .
2. RMSE values related to the covariance, Burg, and modified covariance algorithms concur, showing comparable performance in PSD estimation.
3. The values of p that minimize RMSE are significantly high for observation periods that are longer than 1/128 of the time interval associated with one DVB-T symbol.

To fix an operative range of p of practical use, it has been assumed that RMSE values lower than 3 dB assure acceptable performance in channel power measurement (Fig. 9). A threshold of 3 dB has been applied to the results already obtained, thus achieving a strong reduction in the values of p of interest, with a consequent benefit to the computational burden.

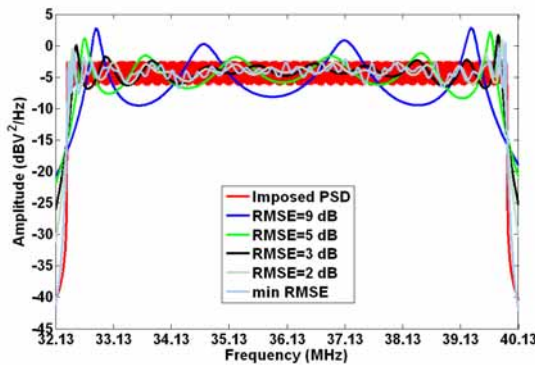


Fig. 9. Estimated PSD versus RMSE.

4.6.2 Fine Optimization

The stage has aimed at fixing the optimal value of p within the operative range established before and comparing the performance granted by the so-optimized covariance, Burg, and modified covariance estimator-based measurement algorithms to that assured by the WOSA-estimator-based algorithm. To reach this goal two figures of merit, σ_C and Δ_C , already defined in paragraph 3, have been minimized.

The obtained values of Δ_C and σ_C and the polynomial order p versus the observation period, which is expressed as a fraction of the time interval associated with one DVB-T symbol, are shown in Fig. 10. An oversampling factor of 3 and a guard interval of 224 μs have been considered. Very similar results have been experienced with a guard interval of 28 μs and two oversampling factors, which are equal to 6 and 12.

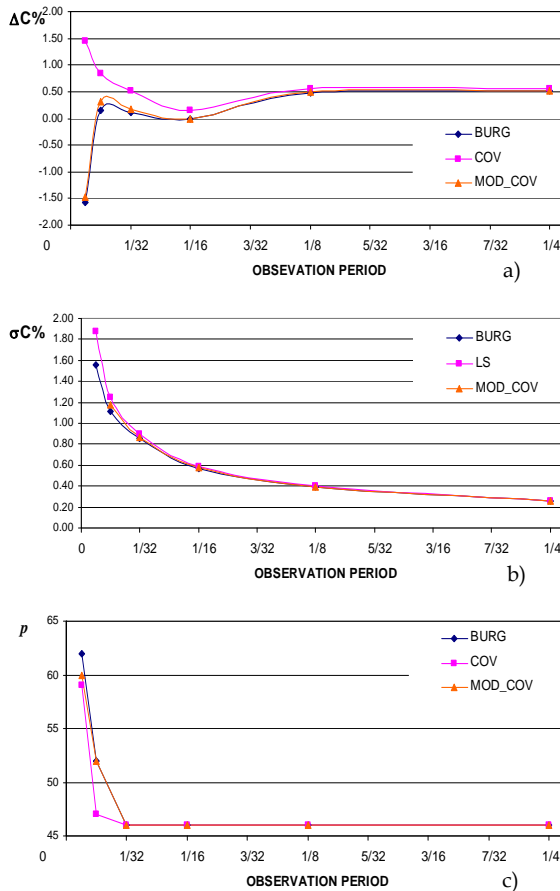


Fig. 10. a) ΔC , b) σC and c) polynomial order p versus the observation period for the considered AR estimator-based measurement algorithms. An oversampling factor equal to 3 and a guard interval equal to 224 μs have been considered.

It is possible to state that the considered AR algorithms grant a very similar performance for both σ_C and Δ_C and that the optimum polynomial order p is equal to 46. In addition, the oversampling factor seems to have no influence; its lowest value (3) is advisable for reducing memory needs.

To fix the minimum hardware requirements of the DAS to be adopted in the experiments on emulated and actual DVB-T signals, the results of which are described in the following, further tests have been carried out. Table 10 gives the estimated σ_C versus the analyzed values of the effective number of bits (ENOB). Observation periods ranging from 1/128 up to 1/4 of the time interval associated with one DVB-T symbol have been considered. σ_C does not seem to be affected by vertical quantization, and the Burg algorithm seems to be more stable if short observation periods are involved.

		ENOB			
Estimators	Observation period	6	7	8	9
BURG	1/128	1.6	1.6	1.5	1.5
	1/64	1.1	1.1	1.1	1.1
	1/32	0.87	0.86	0.86	0.86
	1/16	0.57	0.56	0.57	0.57
	1/8	0.39	0.39	0.39	0.39
	1/4	0.26	0.26	0.26	0.26
COVARIANCE	1/128	1.8	1.9	2.1	1.9
	1/64	1.3	1.3	1.3	1.2
	1/32	0.90	0.90	0.90	0.90
	1/16	0.59	0.58	0.59	0.59
	1/8	0.40	0.40	0.40	0.40
	1/4	0.26	0.26	0.26	0.26
MODIFIED COVARIANCE	1/128	1.7	1.7	1.7	1.7
	1/64	1.2	1.2	1.2	1.2
	1/32	0.87	0.87	0.87	0.86
	1/16	0.58	0.58	0.58	0.58
	1/8	0.40	0.40	0.40	0.40
	1/4	0.26	0.26	0.26	0.26

Table 10. σ_C % versus ENOB for different observation periods.

Computational burden, in terms of the mean processing time on a common Pentium IV computer, has also been quantified.

The results are given in Table 11. It is possible to note that the measurement time peculiar to the Burg-estimator-based measurement algorithm is lower than that taken by the covariance and modified-covariance-estimator-based algorithms for short observation periods.

The Burg-estimator-based measurement algorithm has shown the best tradeoff between metrological performance and measurement time. This is the reason the covariance- and modified covariance estimator-based algorithms have no longer been considered in the subsequent stages of the work.

8k transmission mode and $\Delta=224 \mu\text{s}$						
	Observation period					
Estimator	1/4	1/8	1/16	1/32	1/64	1/128
Burg	0.062	0.036	0.020	0.010	0.008	0.005
Covariance	0.044	0.028	0.018	0.015	0.008	0.015
Modified Covariance	0.052	0.035	0.024	0.021	0.022	0.023
8k transmission mode and $\Delta=28 \mu\text{s}$						
	Observation period					
Estimator	1/4	1/8	1/16	1/32	1/64	1/128
Burg	0.055	0.033	0.016	0.008	0.006	N/A
Covariance	0.039	0.027	0.017	0.015	0.014	N/A
Modified Covariance	0.046	0.040	0.022	0.019	0.020	N/A

Table 11. Computation time in ms versus the observation period.

An emulation stage has been designed and executed with the aim of assessing the performance of the optimized Burg estimator-based measurement algorithm in the presence of a real DAS and comparing the obtained results to those furnished by the optimized WOSA algorithm. Moreover, all results have been compared to those assured by competitive measurement solutions already available on the market.

Thanks to the experience described in the paragraph 3, a suitable measurement station, sketched in Fig. 11, has been designed and setup.

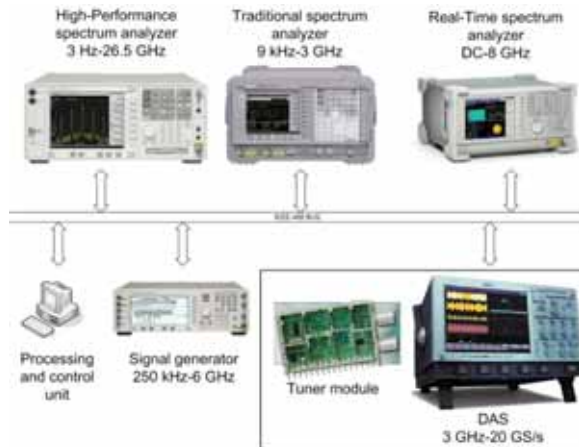


Fig. 11. Measurement station.

It has included:

- a control unit, namely a personal computer (PC);
- a RF signal generator Agilent Technologies E4438C (250 kHz-6 GHz output frequency range), equipped with DVB-T personalities;
- an express spectrum analyzer (ESA) Agilent Technologies E4402B (9 kHz-3 GHz input frequency range);

- a high performance spectrum analyzer (PSA) Agilent Technologies E4440A (3 Hz-26.5 GHz input frequency range);
 - a real-time spectrum analyzer (RSA) Tektronix RSA3408A (DC-8 GHz input frequency range);
 - a DAS LeCroy WavePro 7300A, (3 GHz bandwidth, 20 GS/s maximum sample rate) coupled to the tuner module for digital terrestrial application described in paragraph 3.
- All instruments have been interconnected through an IEEE-488 standard interface bus. The signal generator has provided 8 MHz bandwidth, DVB-T test signals, characterized by a RF center frequency equal to 610 MHz, a nominal total power of -10 dBm and a 64-QAM modulation scheme. Moreover, the same transmission settings considered in the previous stage have been imposed.

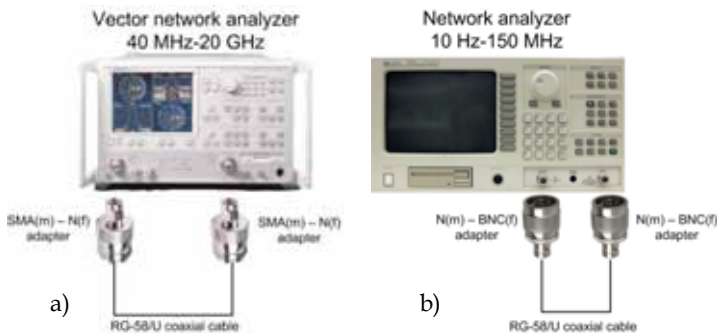


Fig. 12. Measurement bench for the characterization of cables and connectors at a) RF, and b) IF.

A preliminary characterization of cables and connectors utilized in the measurement station has been carried out through the vector network analyzer ANRITSU 37347C (40 MHz-20 GHz input frequency range), equipped with 3650 SMA 3.5 mm calibration kit (Anritsu, 2003), and the spectrum/network analyzer HP 3589A (10 Hz--150 MHz input frequency range) (Agilent, 1991), respectively for RF and IF frequencies. Also the tuner has been characterized.

Different operative conditions of the DAS, in terms of vertical resolution (7- and 8-bit nominal) and observation period (from 1/128 up to 1/4 of the time interval associated with one DVB-T symbol), have been considered; the oversampling factor has been chosen to be equal to 3. For each of them, 100 sample records have been acquired and analyzed both through the Burg- and WOSA-estimator-based measurement algorithms.

The obtained results, which are given in Tables 12-14, have highlighted five conditions.

1. The channel power measures provided by the Burg estimator- based measurement algorithm concur with those furnished by the WOSA-estimator-based algorithm.
2. The channel power measures are influenced by the DAS vertical resolution for both the Burg- and WOSA estimator- based measurement algorithms.
3. Both algorithms exhibit satisfying and comparable repeatability, which is not affected by the DAS vertical resolution and observation period.
- 4) ESA and PSA outcomes concur with the channel power measurement results of the Burg- and WOSA estimator-based measurement algorithms when a DAS resolution of 8 bits is adopted; a confidence level of 95% is considered.

- The outcomes of the RSA operating both in normal conditions and as a spectrum analyzer seem to concur with the channel power measurement results of the Burg- and WOSA estimator-based algorithms only for a DAS resolution of 7 bits; a confidence level of 99% is considered.

8 bit DAS resolution							
		Observation period					
Figure of merit	Guard Interval [μ s]	1/4	1/8	1/16	1/32	1/64	1/128
P_C [μ W]	28	106.41	106.39	106.38	106.52	105.72	N/A
	224	104.87	104.83	104.71	104.68	104.08	102.57
σ_{PC} [μ W]	28	0.75	0.75	0.76	0.77	0.78	N/A
	224	0.74	0.74	0.74	0.75	0.75	0.77
7 bit DAS resolution							
		Observation period					
Figure of merit	Guard Interval [μ s]	1/4	1/8	1/16	1/32	1/64	1/128
P_C [μ W]	28	97.55	97.43	97.31	97.41	96.52	N/A
	224	97.35	97.33	97.12	97.31	96.59	94.92
σ_{PC} [μ W]	28	0.69	0.69	0.69	0.70	0.71	N/A
	224	0.71	0.71	0.71	0.72	0.72	0.73

Table 12. Mean values (P_C) and experimental standard deviations (σ_{PC}) of channel power measures provided by the WOSA estimator-based measurement algorithm. DVB-T settings: 8k transmission mode, 64-QAM modulation scheme.

8 bit DAS resolution							
		Observation Period					
Figure of merit	Guard Interval [μ s]	1/4	1/8	1/16	1/32	1/64	1/128
P_C [μ W]	28	105.65	105.69	105.83	105.90	106.13	N/A
	224	104.30	104.30	104.29	104.27	104.53	104.96
σ_{PC} [μ W]	28	0.74	0.75	0.75	0.76	0.78	N/A
	224	0.74	0.74	0.74	0.74	0.75	0.78
7 bit DAS resolution							
		Observation Period					
Figure of merit	Guard Interval [μ s]	1/4	1/8	1/16	1/32	1/64	1/128
P_C [μ W]	28	96.86	96.76	96.74	96.93	96.99	N/A
	224	96.84	96.83	96.82	96.78	97.01	97.46
σ_{PC} [μ W]	28	0.68	0.68	0.69	0.69	0.71	N/A
	224	0.71	0.71	0.71	0.72	0.72	0.74

Table 13. Mean values (P_C) and experimental standard deviations (σ_{PC}) of channel power measures provided by the Burg estimator-based measurement algorithm. DVB-T settings: 8k transmission mode, 64-QAM modulation scheme.

Instrument	Guard Interval [μ s]	P_C [μ W]	σ_{PC} [μ W]
ESA	28	106.63	0.59
	224	106.24	0.63
PSA	28	106.60	0.64
	224	106.77	0.54
RSA	28	92.68	0.66
	224	93.27	0.61
RSA-SA	28	93.40	0.30
	224	93.69	0.31

Table 14. Mean values (P_C) and experimental standard deviations (σ_{PC}) of channel power measures provided by ESA, VSA, RSA and RSA operating as spectrum analyzer. DVB-T settings: 8k transmission mode, 64-QAM modulation scheme.

A number of experiments on real DVB-T signals have been carried out through the optimized algorithm. The signals have been radiated by one MEDIASET DVB-T multiplexer operating on the UHF 38 (610-MHz RF central frequency) channel.

A simplified measurement station has been adopted. With respect to that used in the emulation stage, the function generator has been replaced by a suitable amplified antenna, the PSA and RSA have been removed, and a power splitter has been added (Angrisani L. et al., 2008). The cables, connectors, and power splitter have been characterized through the aforementioned network analyzers.

The channel power measurement results are summarized in Table 15, and a good agreement can be appreciated.

8k transmission mode, 64-QAM, 28 μ s guard interval UHF Channel 38 (610 MHz)	
	Measured Power [μ W]
WOSA estimator-based measurement algorithm	26.75
<i>Burg</i> estimator-based measurement algorithm	26.92
ESA	26.42

Table 15. Experimental results.

5. Implementation issues in DSP-based meters

In order to evaluate the suitability of these methods to be implemented on real cost effective DSP platform two figures of merit have been taken into account:

- memory requirement, intended as the maximum number of samples to be preserved in the hardware memory;
- computational burden, defined as the number of operations (real additions and real multiplications) to be performed for gaining the desired PSD.

5.1 WOSA estimator

It can be demonstrated that an optimized implementation that is able to reduce the memory requirements would have two requirements.

1. A meter memory that is able to preserve, for the whole measurement time, 2M real samples, which are related to the acquired and overlapped buffers, and 2M complex

samples ($4M$ real samples) for the current and averaged FFT. To prevent additional memory requirements, a computational time to perform the current FFT shorter than $M \cdot (1 - r) \cdot T_s$ is desirable, with T_s being the sampling interval.

2. $M \cdot \log_2(M)$ additions and $M \cdot \log_2(M/2)$ multiplications for each FFT calculation performed on M real samples. It is worth stressing that, to achieve a satisfying frequency resolution in PSD estimation, both K and M should sufficiently be high, with a consequent increase in the memory requirement and computational burden.

As an example, let us consider a DVB-T signal with a center frequency of 36.13 MHz, sampled at 100 MS/s. To achieve a good frequency resolution, i.e., 24 kHz, and good metrological performance in the WOSA estimation (with an overlap ratio of 90% [6], [7]), each FFT has to be calculated on 4096 samples, thus requiring 49152 additions and 45056 multiplications. The storage capability of the meter has to allow at least 24576 real samples to be preserved.

The reduction of memory need and computational burden is possible only if the computational time is lower than $40.96 \mu\text{s}$ (i.e., 4096 samples at 100 MS/s). This is a pressing condition that typically requires the use of expensive multicore platforms.

5.2 Burg estimator

Starting from what Kay and Marple have presented in (Kay & Marple, 1981) and considering the same acquired sequence previously described, it is possible to demonstrate that the minimum number of samples to be stored is $2N + p + 2$, where p is the selected polynomial order, and the $3Np - p^2 - 2N - p$ real additions and $3Np - p^2 - N + 3p$ real multiplications are required for PSD estimation. As for the computational time, the estimation of the current PSD has to take a time interval that is not greater than $N \cdot T_s$, because the whole acquired sequence is involved if real-time operations are pursued.

For $N > 345$, both the computational burden and the required memory depth are higher than those peculiar to the WOSA estimator. To improve this aspect, an optimized implementation called "sequential estimation" that is able to update the PSD estimate whenever a new sample is available can be adopted.

5.3 Sequential Burg estimator

Let us consider (42) for $p = k$, and denote $a_{k,k}$ as K_k .

Making the time dependence explicit, the following relation is obtained:

$$K_k(N) = \frac{2 \sum_{s=k}^N e_{k-1}(s) b_{k-1}^*(s-1)}{\sum_{s=k}^N \left[|e_{k-1}(s)|^2 + |b_{k-1}(s-1)|^2 \right]} \quad (47)$$

where N is the time index. A time-update recursive formulation for (47) is given by

$$K_k(N+1) = K_k(N) + \frac{\left[K_k(N) \left(|e_{k-1}(N)|^2 + |b_{k-1}(N-1)|^2 \right) + 2e_k(N) b_k^*(N-1) \right]}{\sum_{s=k}^N \left[|e_k(s)|^2 + |b_k(s-1)|^2 \right]} \quad (48)$$

Equation (48), combined with (24) and (25), for $k=1, \dots, p$ and initial conditions $e_0(N)=b_0(N)=x_N$, suggests a sequential time-update algorithm for the reflection coefficients. After updating the reflection coefficient K_k , the $k + 1$ parameters $a_{k,1}, a_{k,2}, \dots, a_{k,k}$ and σ_k^2 can be calculated using the Levinson–Durbin recursions. The order of complexity involved is $O(p^2)$, which could significantly worsen the overall computational burden if all coefficients and parameters have to be updated whenever a new sample is available.

Significant computational saving is granted by updating the reflection coefficients $K_k(N)$ at each new sample and all the other parameters after a suitable time interval. More specifically, $9p$ multiplications and $7p$ additions are required to update the reflection coefficients, whereas p^2 multiplications and p^2 additions are needed for all the other parameters.

As for the memory requirement, the minimum number of samples that the sequential implementation requires to be stored is equal to $7p$. The result accounts for p reflection coefficients k_k ; p polynomial coefficients $a_{p,m}$; p forward and p backward prediction errors e_k and b_k , respectively; p coefficients Λ_k and p coefficients Γ_k ; and p estimates of the noise variance σ_k^2 . The obtained value is significantly lower than that required by the non-sequential implementation.

According to the example previously given and considering a value of p equal to 46 (the optimum value previously found), it is possible to assert that 280 samples should be stored in the meter memory, and a computational burden of 360 multiplications and 280 additions should be required to estimate the reflection coefficients.

Hence, it is possible to state that the sequential version of the Burg estimator exhibits better performance than that peculiar to the WOSA estimator and is entitled to be the core of a cost effective DSP-based meter.

6. A cost effective DSP-based DVB-T power meter

In the following the development of a new cost-effective instrument for power measurement in DVB-T systems is proposed. It is based on the improved measurement method sketched in Fig. 13.

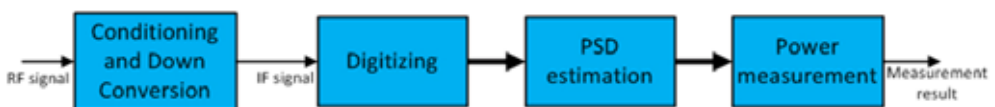


Fig. 13. Simplified block diagram of the proposed measurement method.

After a suitable conditioning and downconversion section, the input signal is digitized and its acquired samples processed in order to estimate its PSD. A proper measurement algorithm, operating on the achieved PSD, finally provides the desired power values.

As for the PSD estimation, the use of Autoregressive (AR) parametric estimators has shown the best trade-off between metrological performance and memory requirements with respect to nonparametric approaches (Angrisani et al., 2009). In addition, as described in (Angrisani et al., 2008-2), efficient implementations of AR parametric PSD estimators have been considered to drastically reduce the measurement time and to limit the memory needs over long observation intervals. A sequential Burg based estimation algorithm has been adopted because it is able to update estimates on data sample by data sample, (Kay & Marple, 1981),

(Marple, 1987) and warrants the best trade-off between computational burden and accuracy, as well as negligible bias and good repeatability.

The core of the proposed instrument is the PSD estimation section that has been implemented on a suitable Field Programmable Gate Array (FPGA) platform. These kinds of digital signal processors are particularly suited for algorithms, such as the sequential implementation of the Burg algorithm, which can exploit the massive parallelism offered by their architecture.

6.1 The hardware

A cost-effective hardware characterizes the meter. It consists of the following sections: (a) the tuner, (b) the analog-to-digital conversion, and (c) the FPGA-based computing platform. A simplified block diagram is depicted in Fig. 14.

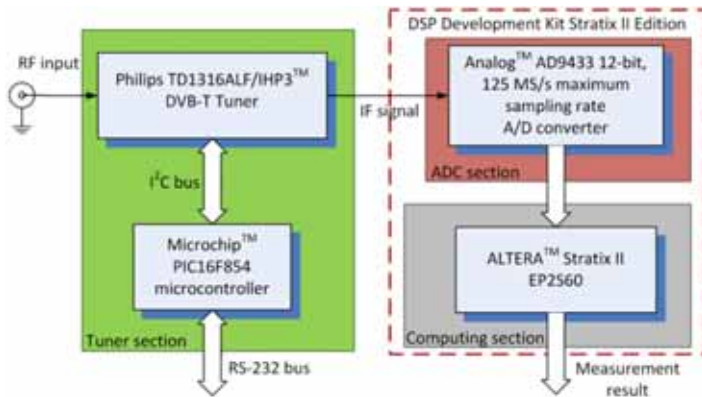


Fig. 14. Simplified block diagram of the proposed DVB-T power meter.

(a) The tuner section down-converts the incoming DVB-T signal, detected by a suitable antenna, to an intermediate frequency (IF) equal to 36.13 MHz. The task is performed by a Philips TD1316ALF/IHP3™ device, which is a single conversion tuner for digital terrestrial applications (NXP, 2006). It is provided with two IF outputs: a narrow-band one, equipped with a surface acoustic wave (SAW) filter and a gain controllable IF-amplifier, and a wideband output without any filter. Both the output circuits are regulated by an internal gain control loop with selectable takeover point settings via I²C bus. An external gain control is also possible if the internal loop is disabled. As far as the narrow-band IF output is concerned, it is possible to select the bandwidth of the SAW filter among 7 MHz and 8 MHz via I²C bus.

All these settings have been controlled and set up by a Microchip™ PIC16F854 microcontroller. It also provides a bus interface conversion between the serial I²C bus of the tuner and a common RS-232 one, allowing a simple connection with PC based environments. In this way, it is possible to set up the DVB-T channel, the SAW filter bandwidth, and the IF amplifier gain.

(b) The analog to digital conversion section is constituted by an Analog™ AD9433. This is a 12-bit monolithic sampling ADC that operates with conversion rates up to 125 MS/s. It is optimized for outstanding dynamic performance in wideband and high IF carrier systems (Analog, 2001).

(c) The computing platform is based on a FPGA chip. In particular the ALTERA™ Stratix II EP2S60 device mounted on the DSP Development Kit Stratix II Edition is considered (Altera, 2007). The chip is a fixed point FPGA that works with operative frequencies from tens of kHz to 400 MHz. This is obtained by using suitable Phase Locked Loops (PLLs) circuits. Other important features of the considered device are the 24176 Adaptive Logic Modules (ALMs), 48352 Adaptive Look-Up Tables (ALUTs), 36 Digital Signal Processing blocks (corresponding to 144 full-precision 18x18-bit multipliers) and 2544192 RAM bits. The typical cost of the considered FPGA chip is of about \$300.

6.2 The firmware

As far as the firmware of the computing platform is concerned, the sequential version of the Burg estimator proposed in (Angrisani et al., 2008-2) and summarized in the block diagram sketched in Fig. 15 is implemented. The firmware operates as follows. After a preliminary initialization phase, not reported in the block diagram, every time a sample is acquired a p -order cycle (i.e. a cycle repeated p times) is started. In each iteration, the estimation of the reflection coefficients (k_i), the σ_i , and the update of the prediction errors is performed. At this

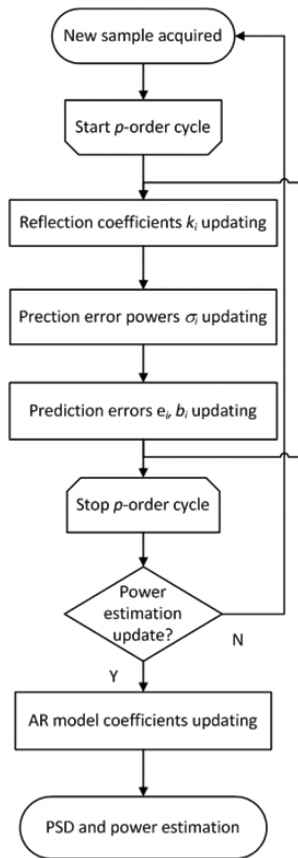


Fig. 15. Block diagram of the implemented FPGA firmware.

stage the user can select if to update the measured power and PSD or not. By updating the desired values of the new coefficients of the p -order model, the estimation of the PSD and channel power is performed, otherwise the p -order cycle begins when a new sample is made available from the ADC.

An order of p equal to 40 has been chosen, and a cascade of 40 sequential blocks implementing the p iterations of the cycle has been realized. The operative frequency of the FPGA device has been set equal to the sampling frequency (100 MS/s). All the implemented blocks warrant a calculation time lower than the sample period (10 ns), thus allowing the real time operation of the instrument. It is worth noting that the firmware architecture realizes a pipeline cascade of computing blocks. This operating way is allowed by the massive parallelism offered by the FPGA architecture. In particular, after a starting latency of 400 ns (i.e. 40 blocks for a sampling time of 10ns) the first measurement result is available. From this time instant on, measurement results are updated each 10 ns.

As far as the hardware resources are concerned, each one of the 40 blocks requires about 4525 ALUTs (Adaptive Look-Up Tables) and 2431 ALMs (Adaptive Logic Modules), thus resulting in a total of 18100 ALUTs and 97240 ALMs for the whole p -order cycle. These values impose the use of a multi-FPGA platform including 4 Stratix II EP2S60 FPGA chips operating in cascade arrangement.

8. References

- Agilent (1991). *HP3589A Operator's Guide*. Hewlett-Packard Company. P/N 03589--90021. Santa Clara (CA), USA.
- Agilent (2001). *E4406A VSA Series Transmitter Tester User's Guide*. Agilent Technol. P/N E4406-90177. Santa Clara (CA), USA.
- Agilent (2003). *AN 1449--2: Fundamentals of RF and Microwave Power Measurements*. Agilent Technologies Inc. EN 5988--9214, Santa Clara (CA), USA.
- Agilent (2003-2). *AN 1303: Spectrum Analyzer Measurements and Noise*. Agilent Technologies Inc. EN 5966--4008, Santa Clara (CA), USA.
- Agilent (2004) *ESA-E Series Spectrum Analyzers Specification Guide*. Agilent Technol. P/N E4401-90472. Santa Clara (CA) USA.
- Agilent (2005). *N1911A and N1912A P-Series Power Meters User's Guide*. Agilent Technol. P/N N1912-90002. Santa Clara (CA) USA.
- Altera (2007). *Stratix II Device Family Handbook*, Altera Corporation. San Jose (CA), USA.
- Analog (2001). 12-bit, 105/125 MSps IF sampling A/D converter AD9433, Analog Devices Inc. Norwood (MA), USA.
- Angrisani L.; D'Apuzzo M. & D'Arco M. (2003). A new method for power measurements in digital wireless communication systems. *IEEE Trans. Instrum. Meas.*, Vol. 52, No. 4, (Aug. 2003) pp. 1097-1106.
- Angrisani L.; Capriglione D.; Ferrigno L. & Miele G. (2006). Reliable and repeatable power measurements in DVB-T systems, *Proceedings IMTC 2006*, pp. 1867-1872, Sorrento, Italy, Apr. 24-27, 2006.
- Angrisani L.; Capriglione D.; Ferrigno L. & Miele G. (2007). Power measurement in DVB-T systems: on the suitability of parametric spectral estimation in DSP-based meters., *Proceedings IMTC 2007*, pp. 1-6, Warsaw, Poland, May 1-3, 2007.

- Angrisani L.; Capriglione D.; Ferrigno L. & Miele G. (2008). Power measurements in DVB-T systems: New proposal for enhancing reliability and repeatability. *IEEE Trans. Instrum. Meas.*, Vol. 57, No. 10, (Oct. 2008) pp. 2108–2117.
- Angrisani L.; Capriglione D.; Ferrigno L. & Miele G. (2008-2) Sequential parametric spectral estimation for power measurements in DVB-T systems, *Proceedings PMTC 2008*, pp. 314–319, Victoria (BC), Canada, May 2008.
- Angrisani L.; Capriglione D.; Ferrigno L. & Miele G. (2009). Power measurement in DVB-T systems: On the suitability of parametric spectral estimation in DSP-based meters. *IEEE Trans. Instrum. Meas.*, Vol. 58, No. 1, (Jan. 2009) pp. 76–86.
- Anritsu (2003). Vector Network Analyzers Technical Data Sheet ANRITSU 37100C/37200C/37300C, Rev. C.
- Burg J. P. (1967). Maximum Entropy Spectral Analysis, *Proceedings of 37th Meeting Soc. Explor. Geophys.*, Oklahoma City (OK), USA, Oct. 31, 1967.
- Daubechies I. (1992). *Ten Lectures on Wavelets*. SIAM, Philadelphia (PA), USA.
- Donoho D. L. & Johnstone I. M. (1994). Ideal spatial adaptation by wavelet shrinkage. *Biometrika*, Vol. 81, No. 3, (Aug. 1994) pp. 425–455.
- ETSI (2004). *EN 300 744: "Digital Video Broadcasting (DVB); Framing structure, channel coding and modulation for digital terrestrial television (V1.5.1)"*. ETSI Std, Sophia Antipolis, France.
- ETSI (2004-2). *TR 101 190: "Digital Video Broadcasting (DVB); Implementation guidelines for DVB terrestrial services; Transmission aspects (V1.2.1)"*. ETSI Std, Sophia Antipolis, France.
- Fischer (2004). *Digital Television – A Practical Guide for Engineers*. Springer-Verlag, ISBN 3540011552, Heidelberg, Germany.
- Jokinen H.; Ollila J. & Aumala O. (2004). On windowing effects in estimating averaged periodograms of noisy signals. *Measurement*, Vol. 28, No. 3, (Oct. 2000) pp. 197–207.
- Kay S. M. & Marple S. L. (1981). Spectrum analysis – A modern perspective. *Proc. IEEE*, Vol. 69, No. 11, (Nov. 1981) pp. 1380–1419.
- Makhoul J. (1975). Linear prediction: A tutorial review. *Proc. IEEE*, Vol. 63, No. 4, (Apr. 1975) pp. 561–580.
- Marple L. (1980). A new autoregressive spectrum analysis algorithm. *IEEE Trans. Acoust., Speech, Signal Process.*, Vol. ASSP-28, No. 4, (Aug. 1980) pp. 441–454.
- Marple S. L. (1987). *Digital Spectral Analysis With Applications*. Prentice-Hall, Englewood Cliffs (NJ), USA..
- Morf M.; Dickinson B.; Kailath T. & Vieira A. (1977). Efficient solution of covariance equations for linear prediction. *IEEE Trans. Acoust., Speech, Signal Process.*, Vol. ASSP-25, No. 5, (Oct. 1977) pp. 429–433.
- Moulin P. (1994), Wavelet thresholding techniques for power spectrum estimation. *IEEE Trans. Signal Process.*, Vol. 42, No. 11, (Nov. 1994) pp. 3126–3136.
- NXP (2006). TD1300A(L)F mk3 Tuner modules for analog and digital terrestrial (OFDM) applications, NXP Semiconductors. Eindhoven, The Netherlands.
- Nuttal A. H. (1976). Spectral analysis of a univariate process with bad data points, via maximum entropy and linear predictive techniques. *Naval Undersea Syst. Cent.*, New London (CT), USA, Tech. Rep. 5303.

- Percival D. B. (1992). Simulating Gaussian random processes with specified spectra. *Comput. Sci. Stat.*, Vol. 24, (1992) pp. 534–538.
- Reljin I.; Reljin B.; Papic V. & Kostic P. (1998). New window functions generated by means of time convolution—Spectral leakage error, *Proceedings of 9th MELECON*, pp. 878–881, Tel-Aviv, Israel, May 18–20, 1998.
- Tektronix (2006). RSA3408A 8 GHz Real-Time Spectrum Analyzer User Manual, Tektronix Inc. 071-1617-01. Beaverton (OR), USA.
- Ulrych T. J. & Clayton R. W. (1976). Time series modelling and maximum entropy. *Phys. Earth Planet. Inter.*, Vol. 12, No. 2/3, (Aug. 1976) pp. 188–200.
- Walden A. T.; Percival D. B. & McCoy E. (1998). Spectrum estimation by wavelet thresholding of multitaper estimators. *IEEE Trans. Signal Process.*, Vol. 46, No. 12, (Dec. 1998) pp. 3153–3165.
- Welch P. D. (1967). The Use of Fast Fourier Transform for the Estimation of Power Spectra: A Method Based on Time Averaging Over Short, Modified Periodograms. *IEEE Transactions on Audio and Electroacoustics*, Vol. AU-15, No. 2, (1967) pp. 70–73.